Bergische Universität Wuppertal

Fachbereich Mathematik und Naturwissenschaften

Lehrstuhl für Angewandte Mathematik
und Numerische Mathematik

Preprint BUW-AMNA 06/02

Andreas Bartel, Stephanie Knorr

# Wavelet-based Adaptive Grids for the Simulation of Multirate Partial Differential-Algebraic Equations

May 2006

http://www.math.uni-wuppertal.de/org/Num/

# WAVELET-BASED ADAPTIVE GRIDS FOR THE SIMULATION OF MULTIRATE PARTIAL DIFFERENTIAL-ALGEBRAIC EQUATIONS

ANDREAS BARTEL AND STEPHANIE KNORR*

**Abstract.** We present an adaptive method to solve biperiodic problems in chip design with widely separated time scales and steep gradients due to digital-like signal structures. Motivated from the example of the switched capacitor filter, we explain the multidimensional signal model and the transformation of network equations to the hyperbolic multirate differential-algebraic system. Then adapted hat-wavelets are introduced to detect the steep gradients. In this way, an adaptive grid is defined for the efficient application of a finite difference method to solve the limit cycle problem.

**Key words.** Electric network, hyperbolic partial differential-algebraic equations, multiscale systems, wavelets, multirate.

**1. Introduction.** To motivate the simulation method presented in this paper, we introduce an industrial test example, the switched capacitor filter (SC-filter) shown in Fig. 1.1 (left). This circuit comprises two major properties we want to focus on, namely widely separated time scales and heterogeneous signal structures. Apart from a slowly varying harmonic input signal (here a sinusoidal $v_{in}$), there are two complementary pulse functions involved (Fig. 1.1, middle), which work on a much faster time scale than the input and cause the angular structure of the output at node 2 (Fig. 1.1, right). After a transient behaviour such a circuit approaches a limit cycle, which needs to be determined in circuit design and is our task in this work.

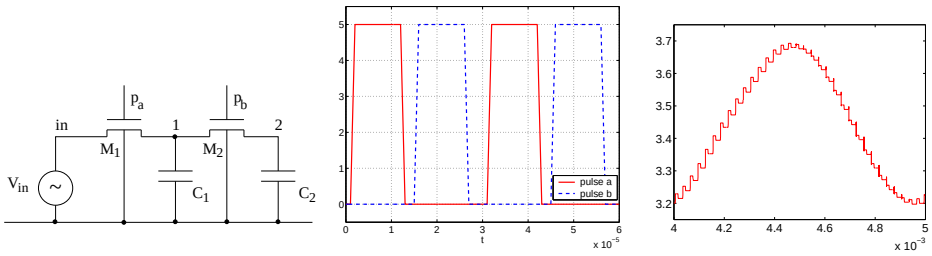


FIG. 1.1. *SC-Filter: Circuit (left), pulses (middle), output node 2 (right).*

To this end, and to treat widely separated time scales efficiently, we use a multidimensional signal model described in the next section. In a numerical integration scheme for the network equations, a very fine grid is necessary to resolve the steep gradients arising due to the pulse functions, where it is of ultimate importance not to skip any pulse. To gain more efficiency, we use the time-frequency localisation property of wavelets for the generation of an adaptive grid, which will be explained in sections 3 and 4. Simulation results for the SC-filter are then presented in section 5.

**2. Multidimensional Signal Model.** To compute the limit cycles for circuits with widely separated time scales, we introduce a corresponding time variable for each occurring scale [1]. The resulting multidimensional representation of a signal yields then a *multivariate function (MVF)*. We illustrate this for a 2-tone quasiperiodic

*Bergische Universität Wuppertal, Fachbereich C - Mathematik, Gaußstr. 20, 42119 Wuppertal, Germany, e-mail: {bartel,knorr}@math.uni-wuppertal.de

signal $x : \mathbb{R} \to \mathbb{R}$, which exhibits amplitude modulation with periodicities $T_1 > T_2$. Its MVF $\hat{x} : \mathbb{R}^2 \to \mathbb{R}$ is derived as follows:

$$x(t) = \Big[1+\tfrac{1}{2}\sin\Big(\tfrac{2\pi}{T_1}t\Big)\Big] \cdot \sin\Big(\tfrac{2\pi}{T_2}t\Big) \quad \rightsquigarrow \quad \hat{x}(t_1,t_2) = \Big[1+\tfrac{1}{2}\sin\Big(\tfrac{2\pi}{T_1}t_1\Big)\Big] \cdot \sin\Big(\tfrac{2\pi}{T_2}t_2\Big), \quad (2.1)$$

such that $x(t) = \hat{x}(t,t)$; both, the signal $x$ and its MVF $\hat{x}$ are depicted in Fig. 2.1.

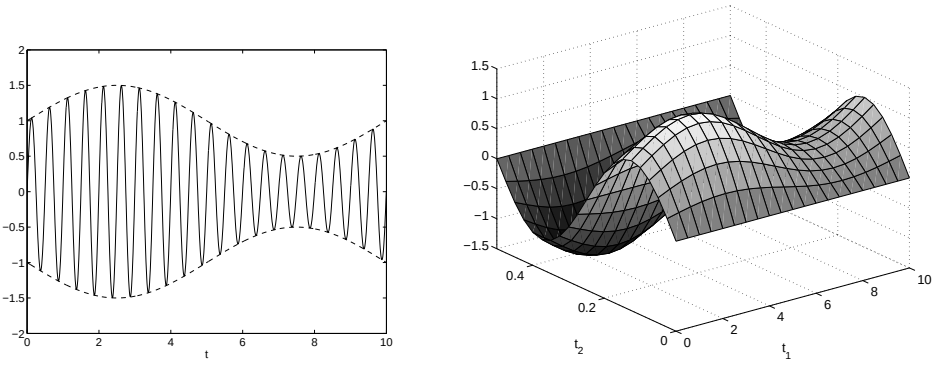


FIG. 2.1. *Multitone signal $x$ (left) and its multivariate function $\hat{x}$ (right).*

In this example, the MVF is periodic in each coordinate direction. Therefore $\hat{x}$ is determined completely on the rectangle of the periodicities $[0, T_1] \times [0, T_2]$ and the diagonal $(t, t) \in \mathbb{R}$ has a representation in that rectangle, which leads to Fig. 2.1 (right). In this way the MVF exhibits just one oscillation in each coordinate direction (the time scales are decoupled) and consequently the signal $\hat{x}$ can be represented with a few number of sampling points. The more the time scales differ ($T_1 \gg T_2$), the more efficient the multidimensional approach becomes, since the structure of the MVF is independent from the ratio $T_1/T_2$ in contrast to the original $x$.

Applying the multidimensional signal model to differential-algebraic network equations [2] leads to a *multirate system of partial differential-algebraic equations (MPDAE)*:

$$\tfrac{\mathrm{d}}{\mathrm{d}t}\,\mathbf{q}(\mathbf{x}(t)) = \mathbf{f}\big(\mathbf{b}(t), \mathbf{x}(t)\big) \quad \rightsquigarrow \quad \frac{\partial \mathbf{q}(\hat{\mathbf{x}})}{\partial t_1} + \frac{\partial \mathbf{q}(\hat{\mathbf{x}})}{\partial t_2} = \mathbf{f}\big(\hat{\mathbf{b}}(t_1,t_2), \hat{\mathbf{x}}(t_1,t_2)\big) \qquad (2.2)$$

with MVFs $\hat{\mathbf{x}}$ of the unknown node potentials and branch currents and $\hat{\mathbf{b}}$ of the input signals; the charges and fluxes are described by $\mathbf{q}$.

In analogy to the underlying ODE-theory, a structural analysis of the MPDAE [4] revealed the characterisation as a PDE-system restricted to a manifold. The hyperbolic type of the inherent PDE allows us to formulate a characteristic system. We are left with systems of differential-algebraic equations for $\bar{\mathbf{x}}_c$

$$\tfrac{\mathrm{d}}{\mathrm{d}\tau}\mathbf{q}(\bar{\mathbf{x}}_c(\tau)) = \mathbf{f}(\hat{\mathbf{b}}(\tau + c, \tau), \bar{\mathbf{x}}_c(\tau)) \quad \text{with} \quad \bar{\mathbf{x}}_c(\tau) = \hat{\mathbf{x}}_c(\tau + c, \tau), \quad \tau \in [0, T_2], \quad (2.3)$$

which exhibit an information transport along straight lines in the direction of the diagonal. To exploit this, we discretise the DAE (2.3) on a characteristic grid [5], which will be described in section 4.

**3. Wavelets for Adaptive Grid Generation.** To detect the steep gradients in the solution for the generation of an adaptive grid, we exploit that the wavelet transform, in contrast to the Fourier transform, not only gives a representation of

the frequency content of a function but also provides information concerning time-localisation:

$$\big(Tf\big)(a,b) = |a|^{-1/2} \int_{\mathbb{R}} f(t)\, \psi\left(\tfrac{t-b}{a}\right) dt. \tag{3.1}$$

The dilation parameter $a \neq 0$ governs the frequency range, whereas the translation parameter $b$ defines the time localisation centre.

To discretise (2.3) along each characteristic curve in the interval $[0, T_2]$, we construct a multiresolution analysis of $L^2([0,T_2])$. Following [3] we set up a biorthogonal basis using hat-functions. The restriction to the bounded interval $[0,T_2]$ is reached by "folding" the basis functions at the edges. Doing this, the biorthogonality is preserved and a hierarchical basis for $L^2([0,T_2])$ is constructed.

Thus we approximate the solution in a subspace $V_J \subset L^2([0,T_2])$, which can be decomposed by the direct sum of a central space $V_0$ spanned by integer translations of a scaling function $\varphi$ and spaces $W_j$ spanned by discrete dilations and translations of the hat-wavelet $\psi$:

$$V_J = V_0 \oplus \bigoplus_{j=0}^{J-1} W_j, \quad W_j = \overline{\operatorname{span}\{\psi_{j,k} \,|\, \psi_{j,k}(\tau) := 2^{j/2}\psi(2^j\tau - k),\, k \in \mathcal{I}_j \subset \mathbb{Z}\}}.$$

To illustrate the time-frequency localisation property of our basis functions, we decompose a pulse function $p : [0,1] \to \mathbb{R}$ (similar to the one occurring in our test example) using the piecewise linear wavelets folded into the pulses domain. Fig. 3.1 shows three plots with the pulse function (dashed line) and the coefficients corresponding to the spaces $V_0$, $W_0$ and $W_1$, respectively. These coefficients are plotted at the locations of the maxima of the corresponding hat-functions (wavelets/scaling functions). Roughly speaking, the coefficients in the left plot (Fig. 3.1) describe coarsely the structure of the pulse, since the maxima of the scaling functions are normalised to 1. The other two sets of coefficients vanish except for the ones, which are needed to resolve the steep gradients. Due to fact that the coefficients are localised in time, we can generate an adaptive grid by 'simply' inspecting the magnitude of the wavelet coefficients.

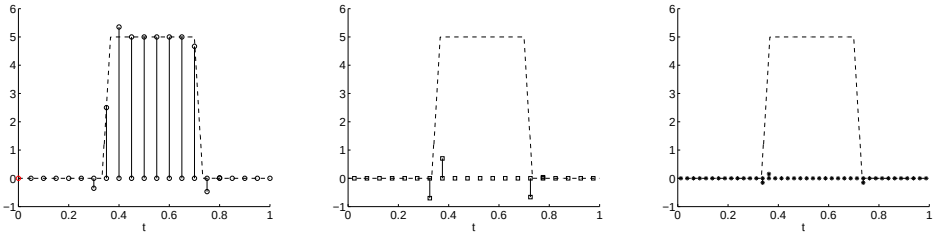


FIG. 3.1. *Decomposition of a pulse with coefficients in $V_0$ (left), $W_0$ (middle) and $W_1$ (right).*

**4. Adaptive Grid Generation.** We have to determine the MPDAE-solution over the rectangle $[0,T_1]\times[0,T_2]$ of the periodicities, which is depicted in Fig. 4.1 (left). The representation of the domain's diagonal, which contains the solution $\mathbf{x}(t) = \hat{\mathbf{x}}(t,t)$ of the original network equations, is indicated by dotted lines; the solid lines show the characteristic curves, along which we will solve system (2.3), only. The periodicity

of the MPDAE-solution $\hat{\mathbf{x}}$ in $t_2$-direction is translated to boundary conditions for the restrictions $\bar{\mathbf{x}}_c$ via interpolation.

For test examples like the SC-filter, the same grid can be used for each characteristic curve, since the locations of the pulses' gradients do not vary in $t_2$-direction. This will clarify when we inspect the simulation results of the SC-filter in the next section. Exploiting this fact, we solve the initial value problem

$$\tfrac{\mathrm{d}}{\mathrm{d}\tau}\mathbf{q}(\mathbf{x}(\tau)) = \mathbf{f}(\mathbf{b}(\tau), \mathbf{x}(\tau)) \quad \text{with} \quad \mathbf{x}(0) = \mathbf{x}_0 \tag{4.1}$$

on the interval $[0, T_2]$, which is just system (2.3) on the first characteristic curve and, of course, far away from the limit cycle. We use a standard algorithm for this integration and transform each component of the obtained solution using the hat-wavelets. The resulting wavelet-coefficients determine an adaptive grid for the respective node on the first characteristic curve, as explained in the previous section. The common grid (suited for all components) is then used on the whole rectangle $[0, T_1] \times [0, T_2]$ and could possibly look like the one depicted in Fig. 4.1 (right).

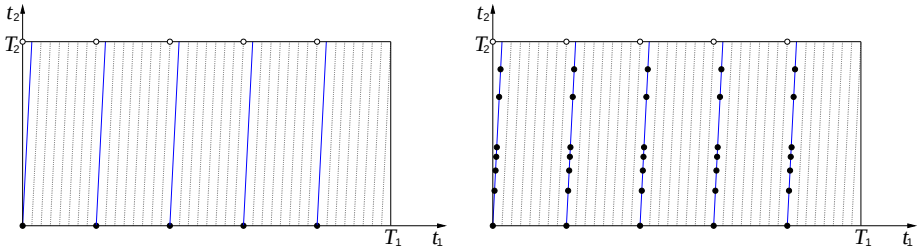


FIG. 4.1. *Characteristic curves (left) and adaptive grid (right).*

The efficiency of this procedure lies in the fact that we only need the time-integration along the first characteristic curve and we do not have to solve for the limit cycle, as we only need the basic structure of the solution to determine an adaptive grid.

Equipped with a grid tailored to the special structure of the solution, we finally solve the DAEs (2.3) using a finite difference discretisation described in [5]. As the equations are only coupled via the interpolation for the boundary conditions, the arising linear system in the Newton iteration is very sparse and can be solved efficiently.

**5. Simulation Results.** The presented method is now applied to simulate the SC-Filter introduced in section 1. This circuit can be described by a set of ordinary differential equations (ODEs); thus the multidimensional signal model leads to multirate partial differential equations (MPDEs).

In this example node 1 "dominates" the grid generation as it is influenced by both pulse functions. The solutions on $[0, T_2]$ for both components and the adaptive grid can be seen in Fig. 5.1 (left) and Fig. 5.2 (left), respectively. The MPDE-solutions (Fig. 5.1 and Fig. 5.2, middle) explain that the same grid can be used for each characteristic curve, as the pulses do not "move" in $t_2$-direction. Last, Fig. 5.1 and Fig. 5.2 show the reconstructed ODE-solutions (right). Comparing the solution for the output node 2 with the exact solution depicted in Fig. 1.1 (right) reveals a very good agreement.

**6. Conclusions.** We presented a method for the adaptive simulation of DAE network equations, which are characterised by widely separated time scales and heterogeneous signal structures. The simulation results are shown for an ODE-example,

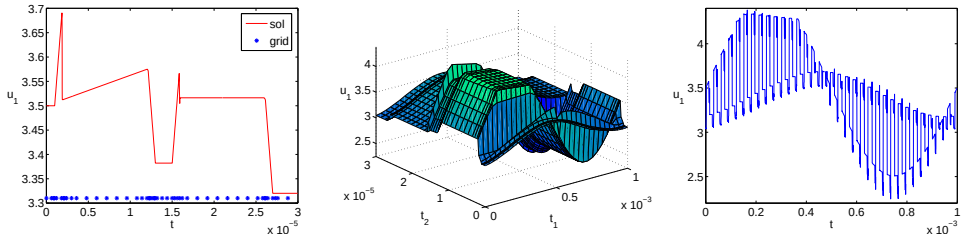


FIG. 5.1. *Node 1: grid generation (left), MPDE-solution (middle), ODE-solution (right).*

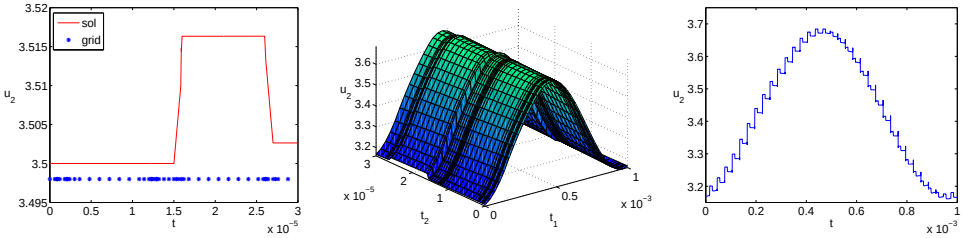


FIG. 5.2. *Node 2: grid generation (left), MPDE-solution (middle), ODE-solution (right).*

as the SC-filter solutions are very well suited to retrace the adaptive grid generation. However, the method works as well for the index-1 case. The next step is to allow a varying grid on different characteristic curves. Furthermore, a full collocation method is aimed at for this class of boundary value problems.

**Acknowledgement.** This work is partially financed by the German ministry BMBF, grant 03GUNAVN, as part of the internal consortium "Numerical Simulation of Multiscale Models for High-Frequency Circuits in Time Domain". The teams of this consortium formed the young researcher's minisymposium on "Multiscale Systems in Refined Network Modeling: Analysis and Numerical Simulation" at GAMM 2006: M. Bodestedt and M. Selva Soto (BMBF grant 03TINAVN by C. Tischendorf), M. Brunk (03JUNAVN by A. Jüngel), T. Sickenberger and R. Winkler (03RONAVN by W. Römisch), and A. Bartel and S. Knorr (03GUNAVN by M. Günther). The GAMM committee is especially acknowledged for the possibility to organize this minisymposium.

## REFERENCES

[1] H.G. Brachtendorf, G.Welsch, R. Laur and A. Bunse-Gerstner, Numerical steady state analysis of electronic circuits driven by multi-tone signals, Electrical Engineering **79**, 103–112 (1996).

[2] P.G. Ciarlet (Ed.), Handbook of Numerical Analysis, Volume XIII: W.H.A. Schilders, E.J.W. ter Maten (Eds.), Numerical Methods in Electronmatgnetics, Elsevier North Holland, Amsterdam (2005).

[3] A. Cohen, I. Daubechies and P. Vial, Wavelets on the Interval and Fast Wavelet Transforms, Applied and Computational Harmonic Analysis **1**, 54–81 (1993).

[4] S. Knorr and M. Günther, Index Analysis of Multirate Partial Differential-Algebraic Systems in RF-Circuits, to appear in: Anile, A.M., Alì, G., Mascali, G. (Ed.), Proceedings of the SCEE 2004 conference, Springer-Verlag, Berlin.

[5] R. Pulch and M. Günther, A method of characteristics for solving multirate partial differential equations in radion frequency application, Appl. Numer. Math. **42**, 397–409 (2002).